Effects of Polytypism on the Thermoelectric Properties of Group-IV Semiconductor Nanowires: A Combination of Density Functional Theory and Boltzmann Transport Calculations

Toru Akiyama, Takato Komoda, Kohji Nakamura, and Tomonori Ito

Department of Physics Engineering, Mie University, 1577 Kurima-Machiya, Tsu 514-8507, Japan

(Received 16 April 2016; published 18 August 2017)

The effects of polytypism on thermoelectric properties of Si and Ge nanowires (NWs) are systematically investigated by using a combination of density functional theory and Boltzmann transport calculations. The calculations for NWs with various polytypes demonstrate that the thermoelectric figure of merit ZT of Si and Ge NWs can be tuned by changing different stacking sequences along the growth direction. In particular, the ZT values of n-type Si and Ge NWs with hexagonal ($2H$) structure at 300 K are significantly larger than ZT of Si and Ge NWs with a cubic ($3C$) structure. The underlying mechanism for the enhanced ZT value in Si NWs with a $2H$ structure compared with a $3C$ structure is attributed by the different Seebeck coefficient depending on the structure, while that in Ge NWs is due to the difference in both the Seebeck coefficient and electrical conductivity. The calculated results offer a way to design high-performance thermoelectric materials by controlling the polytype of NWs.

DOI: 10.1103/PhysRevApplied.8.024014

I. INTRODUCTION

Thermoelectric materials covert directly between heat and electricity, and are expected to play an important role to promote global energy sustainability and energy harvesting. The conversion efficiency of thermoelectric materials is characterized by the dimensionless figure of merit $ZT = S^2\sigma T/\kappa$, where S is the Seebeck coefficient, σ is the electrical conductivity, T is the temperature, κ is the thermal conductivity composed of the electron part κ^e and the lattice part κ^l. Numerous studies have been carried out to obtain a large value of ZT for high conversion efficiency, but these physical properties are coupled with each other, especially in bulk thermoelectric materials: It is difficult to further enhance the ZT values in the bulk phase. Since Hicks and Dresselhaus have proposed a possible route to enhance the ZT value by constructing nanostructures [1], many experimental and theoretical investigations have been extensively explored and have confirmed the feasibility of thermoelectric materials incorporating nanostructures into bulk materials [2–6].

Recently, Si nanowires (NWs) have been demonstrated to possess a high ZT value owing to a reduced thermal conductivity [7,8], and have attracted much attention as promising candidates for thermoelectric materials. It has been experimentally demonstrated that the thermal conductivity of Si NWs can be reduced by diameter [7,9,10] and surface roughness [7,11,12]. On the other hand, several theoretical models have been proposed to explain the decrease of thermal conductivity [13–28], although recent atomistic valence force-field calculations for ultranarrow Si NWs suggested a striking anomalous increase in the thermal conductivity [29]. The impacts of growth direction and doping on the ZT of Si NWs have also been proposed on the basis of electronic structure calculations within density functional theory (DFT) [30]. The impacts of size and isotope concentration on the thermoelectric property of Si NWs have also been investigated by using first-principles tight-binding electronic structure calculation and the Boltzmann transport equation (BTE) [31]. Furthermore, the thermoelectric performance of Ge/Si core-shell NWs has been explored and an excellent thermoelectric performance in Ge/Si NWs due to the remarkable depression of the lattice thermal conductivity has been proposed [32].

Meanwhile, the crystal structure of group-IV NWs is usually characterized by the cubic ($3C$) structure (an *ABCABC*… sequence along the [111] direction), as seen in the bulk phase. However, the incorporation of different stacking sequences induces the suppression of single-crystal NWs along the growth direction. Indeed, the formation of the hexagonal stacking sequence (an *ABAB*... sequence) with cubic-hexagonal heterostructures has been successfully fabricated in Si and Ge NWs [33–35]. Furthermore, the synthesis of Si NWs with a hexagonal ($2H$) structure has been demonstrated by using the chemical vapor deposition [36,37]. The discovery of Si NWs with a hexagonal structure should pertain to other similar materials such as Ge and SiGe: It is expected that elemental group-IV NWs with a different polytype can be realized by controlling the growth conditions. According to theoretical predictions that the band structures of Si and Ge are significantly different between the hexagonal polytypes and $3C$ structure [38–40], the synthesis of novel crystalline phases in group-IV NWs could provide a route to optimizing the thermoelectric properties. The possibility of novel nanowire structures inspires us to examine the effects of polytypism on the thermoelectric properties in group-IV NWs from theoretical viewpoints.

In this paper, we theoretically investigate the effects of polytype on the thermoelectric properties of group-IV NWs on the basis of a combination of DFT and BTE calculations. In order to simulate Si and Ge NWs with various polytypes, we consider various stacking sequences along the [111] and [0001] directions, which correspond to the growth direction of the NWs with cubic and hexagonal structures, respectively. The calculated physical quantities related to thermoelectric properties, such as the Seebeck coefficient and electrical conductivity, are interpreted in terms of electronic band structures obtained by DFT calculations.

II. COMPUTATIONAL DETAILS

Figure 1 depicts the calculation models to clarify the effects of polytype on the thermoelectric properties of NWs. We employ a supercell in which a nanowire is placed with its facets being separated by approximately 7 Å from those of adjacent NWs. The periodicity of these models depends on the polytype of the NWs. The difference between these models can be seen in the size of cubic and hexagonal stacking sequences. In addition to the NWs with a cubic stacking sequence denoted by the $3C$ structure shown in Fig. 1(a), the effects of different ordered stacking sequences are examined by taking account of the NWs, including the hexagonal stacking sequence denoted by $6H$, $4H$, and $2H$ structures shown in Figs. 1(b)–1(d), respectively. We consider H-terminated NWs with a hexagonal shape which is assumed from the crystal symmetry consideration: The structure consisting of hexagonal rings can minimize the number of surface dangling bonds for a certain diameter. The diameters of NWs are almost invariant (around 1.6 and 1.7 nm for Si and Ge NWs, respectively) at a different polytype. Although the size of the NWs is quite a bit smaller than those obtained by the experiments [7,8], qualitative trends of the effects of polytype in thermoelectric properties for realistic NWs could be captured even in NWs with small diameters. To clarify the effects of NW size on thermoelectric properties, we also employ NWs with large diameters (2.5 and 2.6 nm for Si and Ge NWs, respectively) for $3C$ structure.

The geometry optimization and band-structure calculations within the DFT framework are performed using the plane-wave pseudopotential approach with the generalized gradient approximation [41]. To describe electron-ion interactions, we employ norm-conserving pseudopotentials 42]] and Ge $3d$ electrons are treated by partial core corrections [43]. We use the conjugate-gradient technique for both electronic structure calculation and geometry optimization [44–46]. The optimization of geometry is performed until the remaining forces acting on the atoms are less than 5.0×10^{-3} Ry/Å. The valence wave functions are expanded using the plane-wave basis set with a cutoff energy of 16 Ry, and a dense $\mathbf{k}$-point sampling (about 621 points) is set to obtain accurate eigenvalues in the Brillouin zone.

In terms of the group velocity $v_\alpha(i,\mathbf{k})=(1/\hbar)(\partial\varepsilon_{i,\mathbf{k}}/\partial k_\alpha)$, where $\varepsilon_{i,\mathbf{k}}$ is the ith eigenvalue at each $\mathbf{k}$ point obtained by DFT calculations, the energy-projected conductivity tensors $\sigma_{\alpha\beta}(\varepsilon)$ can be defined as

$$\sigma_{\alpha\beta}(\varepsilon) = \frac{e^2}{N_k \Delta\varepsilon} \sum_{i,\mathbf{k}} v_\alpha(i,\mathbf{k}) v_\beta(i,\mathbf{k}) \delta(\varepsilon - \varepsilon_{i,\mathbf{k}}). \quad (1)$$

Here, e is the charge of carriers and N_k is the number of $\mathbf{k}$ points sampled. In this equation, the delta function screens the eigenvalues $\varepsilon_{i,\mathbf{k}}$ whose energy is located within the interval between ε and $\varepsilon + \Delta\varepsilon$, and the sum of $v_\alpha(i,\mathbf{k})v_\beta(i,\mathbf{k})$ is performed for the eigenstates satisfying this condition. From the conductivity tensors in Eq. (1), the electrical conductivity tensors $\sigma_{\alpha\beta}(T,\mu)$, Seebeck coefficient $S(T,\mu)$, and electrical thermal conductivity $\kappa^e(T,\mu)$ as functions of temperature T and electron chemical potential μ (the Fermi energy), can be obtained within the rigid band approach, expressed as

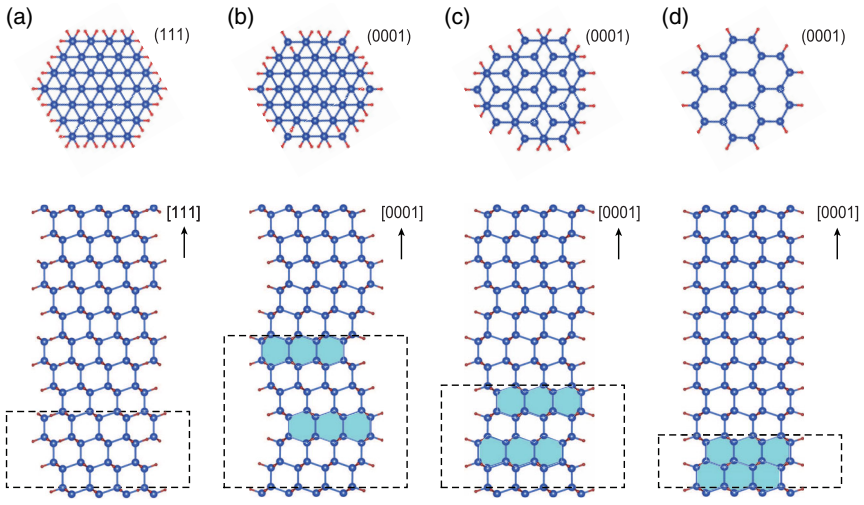

FIG. 1. Top and side views of calculation models for group-IV NWs with (a) $3C$, (b) $6H$, (c) $4H$, and (d) $2H$ structures. Large and small circles represent Si/Ge and H atoms, respectively. The unit cells of slab models along the growth direction are shown by dashed rectangles. The shaded area denotes stacking sequences with a hexagonal symmetry.

$$\sigma_{\alpha\beta}(T,\mu) = \frac{1}{\Omega}\int d\varepsilon \tau \sigma_{\alpha\beta}(\varepsilon)\left[-\frac{\partial f_\mu(T,\varepsilon)}{\partial \varepsilon}\right], \quad (2)$$

$$\nu_{\alpha\beta}(T,\mu) = \frac{1}{eT\Omega}\int d\varepsilon \tau \sigma_{\alpha\beta}(\varepsilon)(\varepsilon-\mu)\left[-\frac{\partial f_\mu(T,\varepsilon)}{\partial \varepsilon}\right], \quad (3)$$

$$S_{\alpha\beta}(T,\mu) = \{\sigma_{i\alpha}(T,\mu)\}^{-1}\nu_{i\beta}, \quad (4)$$

$$\kappa^e_{\alpha\beta}(T,\mu) = \frac{1}{e^2T\Omega}\int d\varepsilon \tau \sigma_{\alpha\beta}(\varepsilon)(\varepsilon-\mu)^2\left[-\frac{\partial f_\mu(T,\varepsilon)}{\partial \varepsilon}\right] - TS_{i\alpha}(T,\mu)\nu_{i\beta}(T,\mu), \quad (5)$$

where Ω is the volume of a unit cell, $f_\mu(\varepsilon)$ is the Fermi distribution function, and τ is the energy- and temperature-dependent relaxation time. In the standard formalism of the elastic scattering of electrons [47,48], the relaxation time is expressed as

$$\tau = \tau_0(T)\left(\frac{\varepsilon}{k_BT}\right)^{r-(1/2)}, \quad (6)$$

where r is related to the charge scattering mechanism: $r=0$ corresponds to the scattering by acoustic phonons, and $r=2$ to the scattering by ionized impurities. τ is constant if $r=1/2$ and τ_0 is independent of temperature. The values of $\tau_0(T)$ at 300 K are obtained by fitting the variation between the measured mobility and carrier concentration for both n- and p-type bulk Si and Ge on the basis of the Drude model for electrical conductivity [49–52]. According to the estimations of scattering matrix elements of Si NWs and the bulk, the relaxation time of Si NWs is approximately 4 times larger than that in bulk Si [30]. Although the use of relaxation time in the bulk phase underestimates the calculated values of ZT, using the relaxation time extrapolated from those of bulk could be reasonable to obtain trends and a qualitative estimation of the thermoelectric properties of NWs. Another concern is the effect of polytype on the relaxation time. In order to check the validity of using constant $\tau_0(T)$ for various polytypes, the difference in scattering potentials depending on the polytype of the NWs is inspected by performing the calculations of B and P atoms in the interior of the NWs. Following the procedure in Ref. [53], the scattering potential ΔV is approximated by the difference in self-consistent local potentials between the NWs with and without impurity. We employ Si and Ge NWs consisting of six bilayers with $3C$, $2H$, and $6H$ structures, and find that the calculated ΔV has a similar profile irrespective of the NW polytype. The difference in plane-averaged values among various NWs is less than 0.06 eV, confirming the intuitive expectation of a similar relaxation time in NWs with a different polytype. The values of $S(T,\mu)$, $\sigma_{\alpha\beta}(T,\mu)$, $\kappa^e_{\alpha\beta}(T,\mu)$ at 300 K for various μ are calculated using the BoltzTraP program [54], where μ is related to the carrier concentration n defined by using the electronic density of states $N(\varepsilon)$ as

$$n = \int d\varepsilon N(\varepsilon) f_\mu(T,\varepsilon). \quad (7)$$

Here, n represents the concentration of charge carriers in a system that is artificially doped by varying the chemical potential μ with a fixed band structure.

There are a number of calculated values reported for the lattice thermal conductivity κ^l of Si and Ge NWs using molecular dynamics [15,18,20–22,25,27,28,32], nonequilibrium Green's functions [16,19], perturbation theory [17], and the BTE for phonon transport [13,14,26,29]. The calculated values of κ^l in NWs are generally smaller than those in bulk phase, but the results strongly depend on the nanowire size and model as well as the calculation procedure. Even for NWs with a relatively large diameter, small values of κ^l less than approximately 5 W/(mK) have been predicted [13]. In this study, we assume $\kappa^l = 1.0$–2.0 (0.75–1.5) W/(mK) for Si (Ge) NWs at a diameter of 1.6 (1.7) nm depending on the polytype. These values are extracted from recent calculated results of lattice thermal conductivity of Si NWs on the basis of the phonon BTE using the ensemble Monte Carlo (MC) technique [26]. The reason why we choose these values is the range of nanowire size treated in Ref. [26], which is close to the diameters of the NWs used in this study. The values of κ^l for Ge NW with a $3C$ structure are determined by considering the difference in the mass number between Si and Ge. To check the validity of using these values for κ^l, we also estimate the lattice thermal conductivity in NWs using diffusive boundary conditions in the BTE for phonons starting from the interatomic force constants obtained by DFT calculations. The calculations are performed within the force constant method using the ShengBTE [55]. The estimated value of κ^l at a diameter of $d_{\mathrm{NW}} = 1.6$ (1.7) nm for Si (Ge) NWs with $3C$ is 2.7 (1.4) W/(mK), which is comparable to those using the ensemble MC technique [26]. It has been reported that surface structure and roughness of NW facets crucially affect the lattice thermal conductivity [18,25,26,28]. We furthermore employ κ^l taking account of the roughness of H-terminated NW facets. As shown in the side views of Fig. 1, the roughness of H-terminated NW facets varies from 0.1 to 0.4 nm, depending on the crystal structure. The value of κ^l takes the highest in the $2H$ structure while the $6H$ structure has the lowest value. Moreover, since the difference between small and large diameters considered in this study is within 1 nm, we also assume these values for NWs with large diameters. The vanishing scattering for long-wavelength phonons that results in an anomalous increase in the thermal conductivity in ultranarrow Si NWs [29] is not taken into account in this study.

III. RESULTS AND DISCUSSION

The calculations of the Seebeck coefficient S, electrical conductivity σ, and electronic thermal conductivity κ^e using various values of r in Eq. (6) demonstrate that there are quantitative differences depending on the scattering type but similar structural dependence are obtained irrespective of r value. Therefore, we henceforth discuss the calculated results using the relaxation time considering the scattering by ionized impurities, which could be suitable to explain the experimental results in Ref. [48]. Figure 2 shows the calculated Seebeck coefficient S, electrical conductivity σ, and electronic thermal conductivity κ^e of p- and n-type Si NWs with $3C$, $6H$, $4H$, and $2H$ structures as a function of carrier concentration at $T = 300$ K [56]. It is found that the amplitudes of the Seebeck coefficient shown in Figs. 2(a) and 2(b) decrease with carrier concentration irrespective of carrier species. The values of S in Si NW with a $3C$ structure obtained in this study are comparable to those using DFT calculations [30]. It should be noted that the value of S depends on the polytype of NWs and takes the smallest value for n-type Si NWs with a $2H$ structure. The enhancement of S in the $2H$ structure with respect to the $3C$ structure is approximately 5%, and is attributed to the difference in density of states depending on the crystal structure [16,31,57,58].

Although recent BTE calculations using the ensemble MC technique have proposed the degradation of electrical conductivity for ultrathin NWs [26], the calculated electrical conductivity using DFT results shown in Figs. 2(c) and 2(d) still exhibits a large electrical conductivity. As expected, both the electrical conductivity [Figs. 2(c) and 2(d)] and the electronic thermal conductivity [Figs. 2(e) and 2(f)] increase as more carriers become available to the transport charge. The calculated σ shown in Figs. 2(c) and 2(d) hardly exhibits a remarkable structural dependence. In particular, it is difficult to distinguish the conductivity difference in the case of high electron concentration owing to the accuracy of group velocity in Eq. (1). In the case of κ^e shown in Figs. 2(e) and 2(f), p-type NWs do not show remarkable structural dependence, whereas n-type NWs with a $2H$ structure exhibit a higher κ^e value compared with the other structures. The structural difference of κ^e in n-type NWs can be interpreted in terms of the band-structure difference shown in Fig. 3. The dispersion of energetically lower conduction bands, which are responsible for transport properties for n-type materials, strongly depends on the polytype of the NWs. Since the energy-projected conductivity tensors in Eq. (1) for n-type NWs are derived from the group velocity of the conduction bands, it is likely

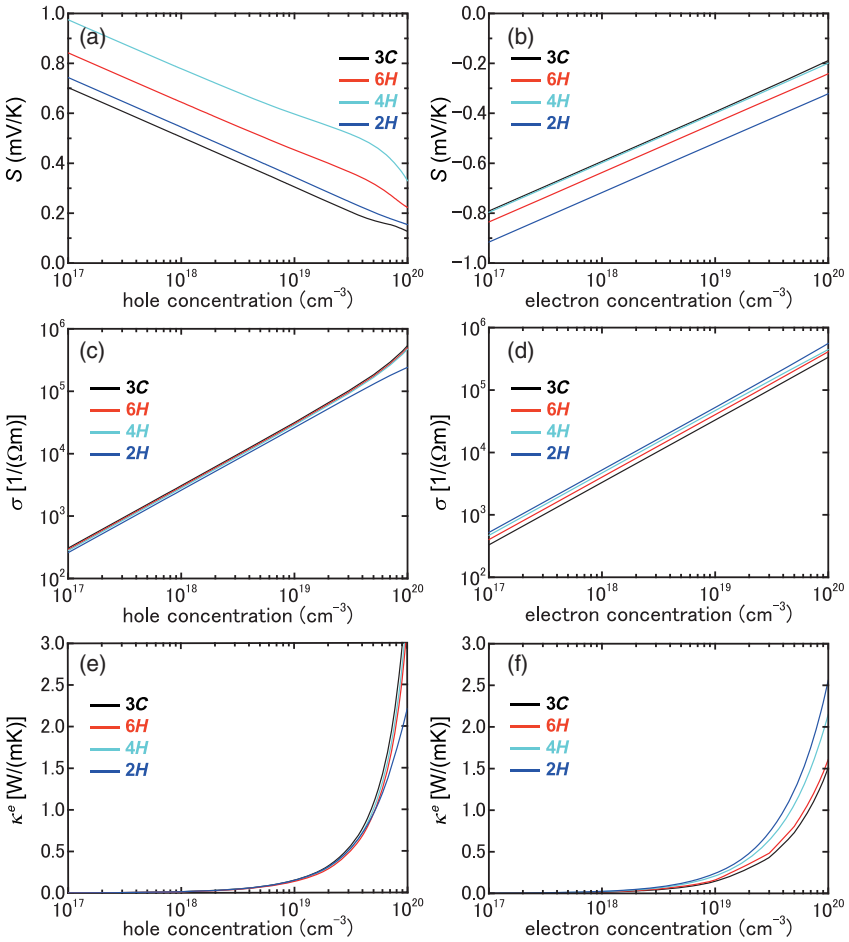

FIG. 2. Calculated (a),(b) Seebeck coefficient S (c),(d) electrical conductivity σ, and (e),(f) electronic thermal conductivity κ^e of Si NWs with for various polytypes as a function of carrier concentration at $T = 300$ K. The left and right panels represent p- and n-type materials, respectively.

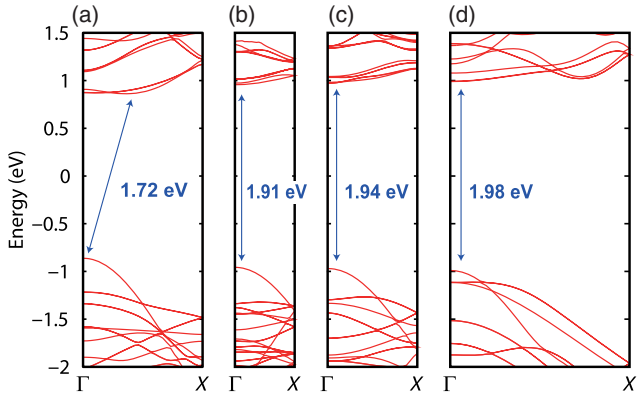

FIG. 3. One-dimensional band structure along the [111] and [0001] directions for Si NWs with (a) $3C$, (b) $6H$, (c) $4H$, and (d) $2H$ structures. The X point in the $3C$ structure corresponds to $[0, 0, 4\pi/(\sqrt{3}a_{3C})]$, where a_{3C} is the lattice constant of the $3C$ structure and the [111] direction is set to the z axis. The X point in the $6H$, $4H$, and $2H$ structure corresponds to $(0, 0, \pi/c)$, where the [0001] direction with the lattice constant c is set to the z axis. The gap energies are also shown. The Fermi level is set to be zero energy.

that the relatively large κ^e value in the $2H$ structure is due to the conduction bands that possess an electron pocket between Γ and X points in addition to the Γ point. As seen in Eqs. (2) and (3), κ^l is more sensitive to the variation of the energy-projected conductivity tensor than σ, leading to the drastic structural dependence in κ^e. However, the structural dependence in κ^e hardly contributes the ZT value since it is weakened in the net thermal conductivity $\kappa = \kappa^e + \kappa^l$ by the lattice thermal conductivity κ^l over the wide range of n less than 1×10^{19} cm^{-3}.

Figure 4 shows the calculated ZT values of Si NWs (at $T = 300$ K) as a function of carrier concentration obtained by using S, σ, and κ^e shown in Fig. 2. It is found that for each NW there is an optimal carrier concentration with a

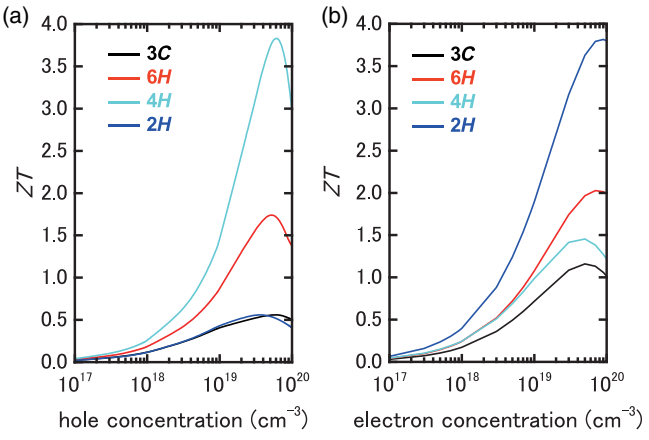

FIG. 4. Calculated ZT as a function of carrier concentration for (a) p-type and (b) n-type Si NWs at $T = 300$ K using the calculated data shown in Fig. 2.

maximum ZT value. For both p- and n-type NWs, the ZT value initially increases with the carrier concentration due to the increase of σ, but the decrease of S and increase of κ^e results in a net decrease of ZT. For p-type NWs, the optimal carrier concentrations range from 3×10^{19} to 5×10^{19} cm^{-3}, depending on the polytype of the NWs. For n-type NWs, the maximum ZT values appear for carrier concentrations larger than 5×10^{19} cm^{-3}. The calculated results demonstrate that the largest ZT value is found to be obtained in $4H$ and $2H$ structures for p- and n-type NWs, respectively, if the optimal carrier concentration is achieved for each structure. As proposed in previous calculations [30,32], the reduction of κ_l enhances the ZT values of the NWs regardless of polytype. However, the largest ZT value of p-type (n-type) NW with $4H$ ($2H$) structure is dominated by the large value of S shown in Figs. 2(a) and 2(b). One of the striking points is that irrespective of the carrier species the incorporation of the hexagonal stacking sequence improves the ZT value of Si NWs with $3C$ structure by more than a factor of 8.

Figure 5 shows the calculated Seebeck coefficient S, electrical conductivity σ, and electronic thermal conductivity κ^e of p- and n-type Ge NWs with $3C$, $6H$, $4H$, and $2H$ structures as a function of carrier concentration at $T = 300$ K [56]. Similar to the case of Si NWs, the amplitudes of the Seebeck coefficient in Ge NWs shown in Figs. 5(a) and 5(b) decrease with the carrier concentration irrespective of the carrier species. It is also found that the value of S depends on the polytype of Ge NWs. The Seebeck coefficient of the $2H$ structure takes the largest value for p-type NWs, while both the $2H$ and $6H$ structures take the smaller values for n-type NWs. The enhancement of S for Ge NWs with the $2H$ structure with respect to the $3C$ structure is approximately 22%.

Both electrical conductivity shown in Figs. 5(c) and 5(d) and electronic thermal conductivity shown in Figs. 5(e) and 5(f) increase with carrier concentration. The calculated σ shown in Fig. 5(c) and κ^e shown in Fig. 5(e) for p-type NWs hardly exhibits remarkable structural dependence. This is because the highest valance bands in these polytypes shown in Fig. 6, which are responsible for transport properties for p-type materials, are similar with each other. In the case of n-type NWs, as shown in Figs. 5(d) and 5(f), Ge NW with a $2H$ structure exhibits higher σ and κ^e values compared with the other structure. The difference in σ and κ^e for n-type NWs can be attributed to the difference in band dispersion for energetically lower conduction bands shown in Fig. 6.

Figure 7 shows the calculated ZT values of Ge NWs (at $T = 300$ K) as a function of carrier concentration obtained by using S, σ, and κ^e shown in Fig. 5. Similar to the case of Si NWs, each Ge NW possesses an optimal carrier concentration with a maximum ZT value. For p-type NWs, the optimal carrier concentrations range from 1×10^{19} to 7×10^{19} cm^{-3}, depending on the polytype of

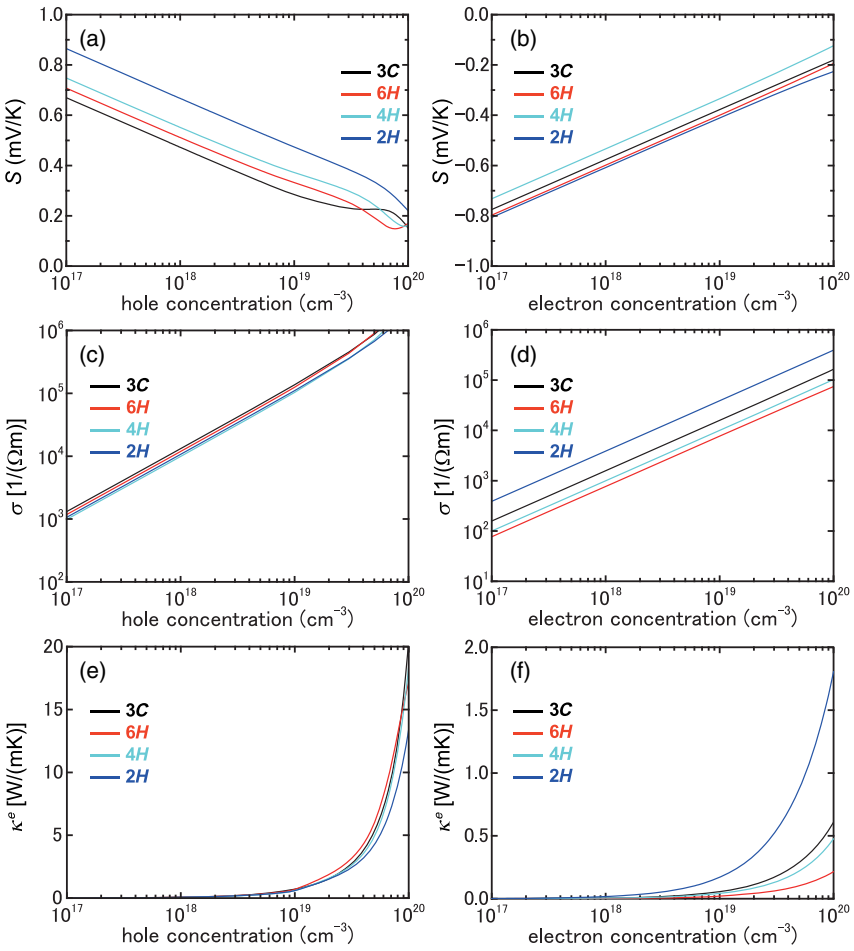

FIG. 5. (a),(b) Seebeck coefficient S; (c),(d) electrical conductivity σ; and (e),(f) electronic thermal conductivity κ^e of Ge NWs for various polytypes as a function of carrier concentration at $T = 300$ K. The left and right panels represent p- and n-type materials, respectively.

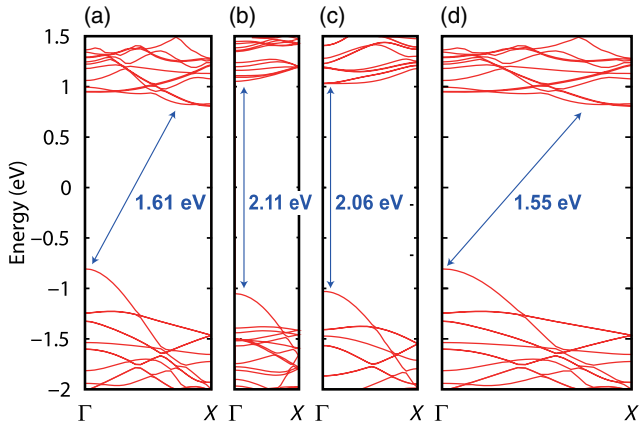

FIG. 6. One-dimensional band structure along the [111] and [0001] directions for Ge NWs with (a) $3C$, (b) $6H$, (c) $4H$, and (d) $2H$ structures. The X point in the $3C$ structure corresponds to $[0, 0, 4\pi/(\sqrt{3}a_{3C})]$, where a_{3C} is lattice constant of $3C$ structure and the [111] direction is set to z axis. The X point in the $6H$, $4H$, and $2H$ structure corresponds to $(0, 0, \pi/c)$, where the [0001] direction with lattice constant c is set to the z axis. The gap energies are also shown. The Fermi level is set to be zero energy.

the NWs. For n-type NWs, the maximum ZT values appear for a carrier concentration larger than 5×10^{19} cm^{-3}. If the optimal carrier concentration is achieved, the largest ZT value can be obtained in the $2H$ structure for both p- and n-type NWs. The largest ZT value in Ge NWs with $2H$ structure is attributed to the highest values of S and σ shown in Figs. 5(a) and 5(d), respectively, in addition to the reduction of κ^l. It is remarkable that the formation of Ge NWs with a $2H$ structure improves the ZT value of Ge NWs with a $3C$ structure by more than a factor of 2. Furthermore, it should be noted that the calculated ZT values of p-type Ge NWs are larger than those of p-type Si NWs owing to the differences in relaxation times and lattice thermal conductivity between Si and Ge. These results suggest that Ge NWs and their alloy (such as SiGe NWs) as well as Si NWs are promising materials for high-performance thermoelectric applications.

In order to check the possibility of larger ZT in NWs with more realistic diameters, we furthermore perform the calculations for Si and Ge NWs with larger diameters for $3C$ structure. Figure 8 shows the calculated ZT of relatively thick Si and Ge NWs (at $T = 300$ K) with the $3C$ structure

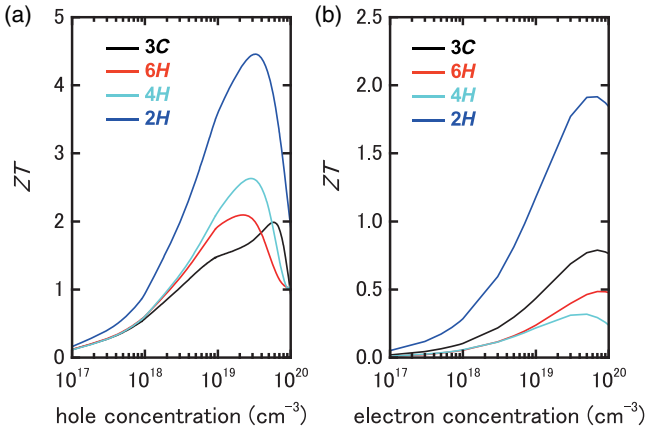

FIG. 7. Calculated ZT as a function of carrier concentration for (a) p-type and (b) n-type Ge NWs at $T = 300$ K using the calculated data shown in Fig. 5.

as a function of carrier concentration obtained by using $S(\varepsilon, T)$, $\sigma(\varepsilon, T)$, and $\kappa^e(\varepsilon, T)$, assuming the scattering by ionized impurities [$r = 2$ in Eq. (6)] [56]. For p-type NWs, the calculated ZT of Si NW with a large diameter is larger than that with a small diameter, while the calculated ZT of Ge NW with a large diameter is smaller than the smaller one. However, the ZT still maintain a large value. For n-type NWs, the calculated ZT of Si and NWs with a larger diameter is comparable to those with a small diameter. Although elaborate and systematic calculations should be necessary to determine the transition point beyond which NWs have bulklike thermoelectric properties, large values in ZT could be at least achieved for NWs with diameters around 3 nm.

Finally, we comment on the effects of relaxation time on thermoelectric properties of NWs. It has been suggested

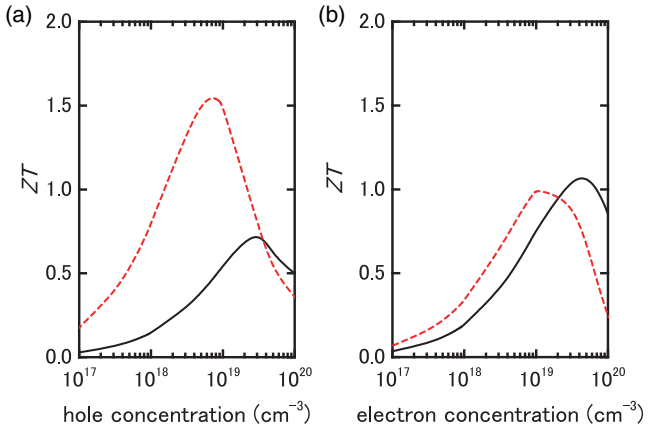

FIG. 8. Calculated ZT as a function of carrier concentration for (a) p-type and (b) n-type Si and Ge NWs with larger diameters (2.5 and 2.6 nm, respectively) for the $3C$ structure at $T = 300$ K using the relaxation time considering the electron scattering by ionized impurities. Solid and dashed lines represent ZT of Si and Ge NWs, respectively.

that the use of bulk relaxation time in the constant-relaxation-time approximation underestimates the ZT values of the NWs [30]. This indicates larger relaxation times in small NWs with respect to bulk values, leading to available ZT values (more than 1) in Si and Ge NWs with a hexagonal stacking sequence. Furthermore, recent non-equilibrium molecular dynamics simulations have demonstrated that owing to the disappearance of favored atom polarization directions the lattice thermal conductivity of Si NWs with twinning superlattices (i.e., twin planes forming a constant spacing) can be reduced by 65% compared with straight ones, which corresponds to NW models considered in this study [27]. Since it has been experimentally reported that such structural modulations are related to the formation of a hexagonal stacking sequence and are able to be introduced in Si NWs by varying growth kinetics [36], it is possible to obtain further a reduction of κ^l and an enhancement of the ZT value by introducing the structural modulations including twinning superlattices. Indeed, by varying the nanowire diameter and growth temperature during the vapor-liquid-solid growth of the NWs, twin-plane superlattices have been successfully fabricated in InP and InAs NWs [59,60]. Moreover, the crystal structure of InP NWs has been controlled by Zn doping: the addition of small amounts of Zn to the vapor phase results in the growth of the NWs with a $3C$ structure [61]. The GaAs NWs grown with C dopants have shown a $3C$ structure without a stacking fault, while the NWs grown without doping exhibit a high density of stacking faults [62]. These kinds of novel nanowire structures could also be achieved in Si and Ge NWs.

IV. SUMMARY

We have employed a combination of the DFT and BTE calculations to examine the effects of the polytype on the thermoelectric properties of Si and Ge NWs. We have found that by changing different stacking sequences along the growth direction, it is possible to tune the thermoelectric figure of merit of Si and Ge NWs. It is also noteworthy that the calculated ZT values of n-type Si and Ge NWs with a $2H$ structure are significantly larger than those with a conventional $3C$ structure. The enhancement of ZT values in n-type NWs with a $2H$ structure in Si NWs is mainly attributed to the different value of the Seebeck coefficient depending on the structure of the NWs, while the difference in both the Seebeck coefficient and the electrical conductivity depending on the structure of the NWs contributes to the thermoelectric properties of Ge NWs. Although the results obtained in this study should be checked from various viewpoints, including the effects of nanowire size and surface structures of nanowire facets, our results will stimulate experimental and theoretical efforts to design high-performance thermoelectric materials by controlling the polytype of the NWs.

ACKNOWLEDGMENTS

This work was supported in part by Grant-in-Aid for Scientific Research Grants No. JP17K05056, No. JP16K04962, and No. JP16H06418 from the Japan Society for the Promotion of Science. T. A. would like to thank the Research Foundation for the Electrotechnology of Chubu for financial support. Computations were performed at the Research Center for Computational Science (National Institutes of Natural Sciences) and the Research Institute for Information Technology (Kyushu University).

[1] L. D. Hicks and M. S. Dresselhaus, Effect of quantum-well structures on the thermoelectric figure of merit, Phys. Rev. B **47**, 12727 (1993).

[2] Rama Venkatasubramanian, Edward Siivola, Thomas Colpitts, and Brooks O'Quinn, Thin-film thermoelectric devices with high room-temperature figures of merit, Nature (London) **413**, 597 (2001).

[3] T. C. Harman, P. J. Taylor, M. P. Walsh, and B. E. LaForge, Quantum dot superlattice thermoelectric materials and devices, Science **297**, 2229 (2002).

[4] Pierre F. P. Poudeu, Jonathan D'Angelo, Huijun Kong, Adam Downey, Jarrod L. Short, Robert Pcionek, Timothy P. Hogan, Ctirad Uher, and Mercouri G. Kanatzidis, Nanostructures versus solid solutions: Low lattice thermal conductivity and enhanced thermoelectric figure of merit in $Pb_{9.6}Sb_{0.2}Te_{10-x}4Se_x$ bulk materials, J. Am. Chem. Soc. **128**, 14347 (2006).

[5] Bed Poudel, Qing Hao, Yi Ma, Yucheng Lan, Austin Minnich, Bo Yu, Xiao Yan, Dezhi Wang, Andrew Muto, Daryoosh Vashaee, Xiaoyuan Chen, Junming Liu, Mildred S. Dresselhaus, Gang Chen, and Zhifeng Ren, High-thermoelectric performance of nanostructured bismuth antimony telluride bulk alloys, Science **320**, 634 (2008).

[6] Yucheng Lan, Austin Jerome Minnich, Gang Chen, and Zhifeng Ren, Enhancement of thermoelectric figure-of-merit by a bulk nanostructuring approach, Adv. Funct. Mater. **20**, 357 (2010).

[7] Allon I. Hochbaum, Renkun Chen, Raul Diaz Delgado, Wenjie Liang, Erik C. Garnett, Mark Najarian, Arun Majumdar, and Peidong Yang, Enhanced thermoelectric performance of rough silicon nanowires, Nature (London) **451**, 163 (2008).

[8] Akram I. Boukai, Yuri Bunimovich, Jamil Tahir-Kheli, Jen-Kan Yu, William A. Goddard III, and James R. Heath, Silicon nanowires as efficient thermoelectric materials, Nature (London) **451**, 168 (2008).

[9] Deyu Li, Yiying Wu, Philip Kim, Li Shi, Peidong Yang, and Arun Majumdar, Thermal conductivity of individual silicon nanowires, Appl. Phys. Lett. **83**, 2934 (2003).

[10] Joseph P. Feser, Jyothi S. Sadhu, Bruno P. Azeredo, Keng H. Hsu, Jun Ma, Junhwan Kim, Myunghoon Seong, Nicholas X. Fang, Xiuling Li, Placid M. Ferreira, Sanjiv Sinha, and David G. Cahill, Thermal conductivity of silicon nanowire arrays with controlled roughness, J. Appl. Phys. **112**, 114306 (2012).

[11] Kedar Hippalgaonkar, Baoling Huang, Renkun Chen, Karma Sawyer, Peter Ercius, and Arun Majumdar, Fabrication of microdevices with integrated nanowires for investigating low-dimensional phonon transport, Nano Lett. **10**, 4341 (2010).

[12] Jongwoo Lim, Kedar Hippalgaonkar, Sean C. Andrews, Arun Majumdar, and Peidong Yang, Quantifying surface roughness effects on phonon transport in silicon nanowires, Nano Lett. **12**, 2475 (2012).

[13] Natalio Mingo, Liu Yang, Deyu Li, and Arun Majumdar, Predicting the thermal conductivity of Si and Ge nanowires, Nano Lett. **3**, 1713 (2003).

[14] David Lacroix, Karl Joulain, Damian Terris, and Denis Lemonnier, Monte Carlo simulation of phonon confinement in silicon nanostructures: Application to the determination of the thermal conductivity of silicon nanowires, Appl. Phys. Lett. **89**, 103104 (2006).

[15] Inna Ponomareva, Deepak Srivastava, and Madhu Menon, Thermal conductivity in thin silicon nanowires: Phonon confinement effect, Nano Lett. **7**, 1155 (2007).

[16] Jian Wang and Jian-Sheng Wang, Dimensional crossover of thermal conductance in nanowires, Appl. Phys. Lett. **90**, 241908 (2007).

[17] Pierre Martin, Zlatan Aksamija, Eric Pop, and Umberto Ravaioli, Impact of Phonon-Surface Roughness Scattering on Thermal Conductivity of Thin Si Nanowires, Phys. Rev. Lett. **102**, 125503 (2009).

[18] Davide Donadio and Giulia Galli, Atomistic Simulations of Heat Transport in Silicon Nanowires, Phys. Rev. Lett. **102**, 195901 (2009).

[19] Troels Markussen, Antti-Pekka Jauho, and Mads Brandbyge, Electron and phonon transport in silicon nanowires: Atomistic approach to thermoelectric properties, Phys. Rev. B **79**, 035415 (2009).

[20] Davide Donadio and Giulia Galli, Temperature dependence of the thermal conductivity of thin silicon nanowires, Nano Lett. **10**, 847 (2010).

[21] Ling Liu and Xi Chen, Effect of surface roughness on thermal conductivity of silicon nanowires, J. Appl. Phys. **107**, 033501 (2010).

[22] Takumi Saegusa, Koji Eriguchi, Kouichi Ono, and Hiroaki Ohta, Molecular dynamics evaluation of thermal transport in naked and oxide-coated silicon nanowires, Jpn. J. Appl. Phys. **49**, 095204 (2010).

[23] Yi-Ray Chen, Ming Shan Jeng, Ya Wen Chou, and Chang Chung Yang, Molecular dynamics simulation of the thermal conductivities of Si nanowires with various roughnesses, Comput. Mater. Sci. **50**, 1932 (2011).

[24] Mathieu Luisier, Investigation of thermal transport degradation in rough Si nanowires, J. Appl. Phys. **110**, 074510 (2011).

[25] Yuping He and Giulia Galli, Microscopic Origin of the Reduced Thermal Conductivity of Silicon Nanowires, Phys. Rev. Lett. **108**, 215901 (2012).

[26] E. B. Ramayya, L. N. Maurer, A. H. Davoody, and I. Knezevic, Thermoelectric properties of ultrathin silicon nanowires, Phys. Rev. B **86**, 115328 (2012).

[27] Shiyun Xiong, Yuriy A. Kosevich, K. Sääskilahti, Yuxiang Ni, and Sebastian Volz, Tunable thermal conductivity in silicon twinning superlattice nanowires, Phys. Rev. B **90**, 195439 (2014).

[28] T. Zushi, K. Ohmori, K. Yamada, and T. Watanabe, Effect of a SiO_2 layer on the thermal transport properties of $\langle 100 \rangle$ Si nanowires: A molecular dynamics study, Phys. Rev. B **91**, 115308 (2015).

[29] Hossein Karamitaheri, Neophytos Neophytou, and Hans Kosina, Anomalous diameter dependence of thermal transport in ultra-narrow Si nanowires, J. Appl. Phys. **115**, 024302 (2014).

[30] Trinh T. M. Vo, Andrew J. Williamson, Vincenzo Lordi, and Giulia Galli, Atomistic design of thermoelectric properties of silicon nanowires, Nano Lett. **8**, 1111 (2008).

[31] Lihong Shi, Donglai Yao, Gang Zhang, and Baowen Li, Size dependent thermoelectric properties of silicon nanowires, Appl. Phys. Lett. **95**, 063102 (2009).

[32] Xin Chen, Yanchao Wang, and Yanming Ma, High thermoelectric performance of Ge/Si core-shell nanowires: First-principles prediction, J. Phys. Chem. C **114**, 9096 (2010).

[33] Jordi Arbiol, Billel Kalache, Pere Roca i Cabarrocas, Joan Ramon Morante, and Anna Fontcuberta i Morral, Influence of Cu as a catalyst on the properties of silicon nanowires synthesized by the vapour-solid-solid mechanism, Nanotechnology **18**, 305606 (2007).

[34] Jordi Arbiol, Anna Fontcuberta i Morral, Sónia Estradé, Francesca Peiró, Billel Kalache, Pere Roca i Cabarrocas, and Joan Ramon Morante, Influence of the (111) twinning on the formation of diamond cubic/diamond hexagonal heterostructures in Cu-catalyzed Si nanowires, J. Appl. Phys. **104**, 064312 (2008).

[35] Subhajit Biswas, Jessica Doherty, Dipanwita Majumdar, Tandra Ghoshal, Kamil Rahme, Michelle Conroy, Achintya Singha, Michael A. Morris, and Justin D. Holmes, Diameter-controlled germanium nanowires with lamellar twinning and polytypes, Chem. Mater. **27**, 3408 (2015).

[36] Dunwei Liu and Xiaohuaand Wang, Kinetically-induced hexagonality in chemically grown silicon nanowires, Nano Res. **2**, 575 (2009).

[37] A. Fontcuberta Morral, J. Arbiol, J. Prades, A. Cirera, and J. Morante, Synthesis of silicon nanowires with wurtzite crystalline structure by using standard chemical vapor deposition, Adv. Mater. **19**, 1347 (2007).

[38] C. Raffy, J. Furthmüller, and F. Bechstedt, Properties of hexagonal polytypes of group-IV elements from first-principles calculations, Phys. Rev. B **66**, 075201 (2002).

[39] Florian Kiefer, Viktor Hlukhyy, Antti J. Karttunen, Thomas F. Fassler, Christian Gold, Ernst-Wilhelm Scheidt, Wolfgang Scherer, Johanna Nylen, and Ulrich Haussermann, Synthesis, structure, and electronic properties of 4*H*-germanium, J. Mater. Chem. **20**, 1780 (2010).

[40] Amrit De and Craig E. Pryor, Electronic structure and optical properties of Si, Ge and diamond in the lonsdaleite phase, J. Phys. Condens. Matter **26**, 045801 (2014).

[41] John P. Perdew, Kieron Burke, and Matthias Ernzerhof, Generalized Gradient Approximation Made Simple, Phys. Rev. Lett. **77**, 3865 (1996).

[42] N. Troullier and Jos Luriaas Martins, Efficient pseudopotentials for plane-wave calculations, Phys. Rev. B **43**, 1993 (1991).

[43] Steven G. Louie, Sverre Froyen, and Marvin L. Cohen, Nonlinear ionic pseudopotentials in spin-density-functional calculations, Phys. Rev. B **26**, 1738 (1982).

[44] M. Tsukada *et al.*, Computer program package TAPP, University of Tokyo, Tokyo, Japan (2017).

[45] Jun Yamauchi, Masaru Tsukada, Satoshi Watanabe, and Osamu Sugino, First-principles study on energetics of c-BN(001) reconstructed surfaces, Phys. Rev. B **54**, 5586 (1996).

[46] Hiroyuki Kageshima and Kenji Shiraishi, Momentum-matrix-element calculation using pseudopotentials, Phys. Rev. B **56**, 14985 (1997).

[47] K. Durczewski and M. Ausloos, Nontrivial behavior of the thermoelectric power: Electron-electron versus electron-phonon scattering, Phys. Rev. B **61**, 5303 (2000).

[48] T. Okuda, K. Nakanishi, S. Miyasaka, and Y. Tokura, Large thermoelectric response of metallic perovskites: $Sr_{1-x}La_xTiO_3$ ($0 < \sim x < \sim 0.1$), Phys. Rev. B **63**, 113104 (2001).

[49] D. B. Cuttriss, Relation between surface concentration and average conductivity in diffused layers in germanium, Bell Syst. Tech. J. **40**, 509 (1961).

[50] L. S. Stilbans, O. A. Golikova, and B. Y. Moizhez, Hole mobility of germanium as a function of concentration and temperature, Sov. Phys. Solid State **3**, 2259 (1962).

[51] Sheng S. Li and W. Robert Thurber, The dopant density and temperature dependence of electron mobility and resistivity in *n*-type silicon, Solid State Electron. **20**, 609 (1977).

[52] J. M. Dorkel and Ph. Leturcq, Carrier mobilities in silicon semi-empirically related to temperature, doping and injection level, Solid State Electron. **24**, 821 (1981).

[53] Vincenzo Lordi, Paul Erhart, and Daniel Åberg, Charge carrier scattering by defects in semiconductors, Phys. Rev. B **81**, 235204 (2010).

[54] Georg K. H. Madsen and David J. Singh, BOLTZTRAP. A code for calculating band-structure dependent quantities, Comput. Phys. Commun. **175**, 67 (2006).

[55] Wu Li, Jesús Carrete, Nebil A. Katcho, and Natalio Mingo, SHENGBTE: a solver of the Boltzmann transport equation for phonons, Comput. Phys. Commun. **185**, 1747 (2014).

[56] See Supplemental Material at http://link.aps.org/supplemental/10.1103/PhysRevApplied.8.024014 for calculated thermoelectric properties (S, σ, κ^e, and ZT as a function of carrier concentration) of Si and Ge NWs with 3*C*, 6*H*, 4*H*, and 2*H* structures using different treatments of relaxation time, and those of Si and Ge NWs with large diameters for 3*C* structure.

[57] G. D. Mahan and J. O. Sofo, The best thermoelectric, Proc. Natl. Acad. Sci. U.S.A. **93**, 7436 (1996).

[58] T. E. Humphrey and H. Linke, Reversible Thermoelectric Nanomaterials, Phys. Rev. Lett. **94**, 096601 (2005).

[59] P. Caroff, K. A. Dick, J. Johansson, M. E. Messing, K. Deppert, and L. Samuelson, Controlled polytypic and twin-plane superlattices in III–V nanowires, Nat. Nanotechnol. **4**, 50 (2009).

[60] Rienk E. Algra, Marcel A. Verheijen, Magnus T. Borgstrom, Lou-Fe Feiner, George Immink, Willem J. P. van Enckevort, Elias Vlieg, and Erik P. A. M. Bakkers, Twinning superlattices in indium phosphide nanowires, Nature (London) **456**, 369 (2008).

[61] Keitaro Ikejiri, Fumiya Ishizaka, Katsuhiro Tomioka, and Takashi Fukui, Bidirectional growth of indium phosphide nanowires, Nano Lett. **12**, 4770 (2012).

[62] O. Salehzadeh and S. P. Watkins, Effect of carbon tetrabromide on the morphology of GaAs nanowires, Nanotechnology **22**, 165603 (2011).